Construction and Building Materials 124 (2016) 363–372

Contents lists available at ScienceDirect

Construction and Building Materials

journal homepage: www.elsevier.com/locate/conbuildmat

An investigation into the thermal conductivity of hydrating sprayed concrete

Shuangxin Li [a], Benoît Jones [b,*], Roger Thorpe [b], Martin Davis [b]

[a] School of Civil Engineering, Harbin Institute of Technology, 150001 China
[b] School of Engineering, University of Warwick, CV4 7AL, UK

HIGHLIGHTS

- Early age thermal conductivity is mainly influenced by free water content.
- Mature age thermal conductivity is mainly influenced by porosity.
- Thermal conductivity is found to exponentially vary with density.

ARTICLE INFO

Article history:
Received 10 October 2013
Received in revised form 28 June 2016
Accepted 15 July 2016

Keywords:
Sprayed concrete
Thermal conductivity
Transient method
Mathematical stimulation

ABSTRACT

Information about the thermal conductivity of sprayed concrete is useful for calibration exercises using sprayed panels, where heat flows need to be estimated, and future enhancements to the method to include estimates of concrete temperature across the thickness of the lining. However, the necessary information about thermal conductivity of sprayed concrete is rare, and no information about the early age thermal conductivity of sprayed concrete has been found. The thermal conductivity of sprayed concrete aging from five hours after casting to 20 days was continuously measured by a transient method. Thermal conductivity was found to be higher than expected at early age and decreased to the mature value as the concrete cured. Based on these results it is hypothesized that early age thermal conductivity is mainly influenced by free water content, while at a mature stage the key determinants are the structural features of the cement matrix. Thermal conductivity is discovered to have an exponential relationship with density, regardless of mix constituents. A convenient numerical approach is proposed to estimate thermal conductivity for concretes and its accuracy has been verified by data from tests on a wide range of concretes with density ranging from 0.2 g/cm^3 to 2.5 g/cm^3.

1. Introduction

The new method of strength monitoring using thermal imaging, known as SMUTI, provides a system that measures the surface temperature of the sprayed concrete tunnel lining to assess the curing of concrete [1]. The temperature history is then used to calculate compressive strength using an Arrhenius equation-based time-stepping algorithm [2]. This technique will especially benefit sprayed concrete tunnel construction since it will improve work efficiency and safety by reducing the need for a large amount of in situ testing, removing the need to access the face area of the tunnel, and by providing the compressive strength of the whole tunnel lining and not just discrete areas.

Although not essential to SMUTI, information about the thermal conductivity of sprayed concrete is useful for calibration exercises using sprayed panels, where heat flows need to be estimated, and future enhancements to the method to include estimates of concrete temperature across the thickness of the lining. However, the necessary information about thermal conductivity of sprayed concrete is rare, and no information about the early age thermal conductivity of sprayed concrete has been found. Thus, the aim of this paper is: (1) to prepare concrete identical with the one used in practice; (2) experimentally determine the effective thermal conductivity (ETC) of sprayed concrete; (3) establish a numerical model for evaluating ETC of concrete; (4) validate the numerical model with experimental results; (5) evaluate the effect of steel-fiber reinforcement on ETC.

* Corresponding author.
E-mail address: b.d.jones@warwick.ac.uk (B. Jones).

http://dx.doi.org/10.1016/j.conbuildmat.2016.07.091
0950-0618/

1.1. Sprayed concrete

Sprayed concrete can be traced back to 1911 when it was known as "gunite" [3]. It is pneumatically projected through a nozzle where a chemical accelerator is added [4]. In this way layers may be built up to form a tunnel lining. Sprayed concrete has a different mix design compared to conventional in situ poured concrete. Fine particles (fine aggregate and cement) are dominant in the mix, cement content is between 400 and 450 kg/m^3, and often silica fume is added. The fraction of coarse aggregates greater than 4 mm, usually with a maximum size of 8–10 mm, is only approximately one quarter of the mass of sand (<4 mm), which is the opposite of what is normal for conventional concrete. Thus, a higher pump-ability and workability is achieved with very little segregation or bleeding. Chemicals are used to control hydration of cement (retarders and alkali-free accelerators) or adjust water content (superplasticisers). Sometimes pozzolanic or/and latent hydraulic binding material is added to improve certain properties in the plastic and/or hardened state, and steel reinforcement (wire mesh, bars or fibers) is used to increase the flexural strength and control cracking. Today, sprayed concrete is widely used in underground construction, requiring a fast setting and adequate early-age compressive strength to provide structural support.

In tunnel construction, the development of the early age compressive strength of sprayed concrete is critical not only because of its structural function and the need to support the ground before continuing excavation, but also for protection of the workers from falling ground or indeed falling sprayed concrete. However, the currently recommended strength testing methods, which are penetration needle tests and stud driving method [5], have their inherent defects: difficult and time-consuming operation, small examined areas and scattered data. Usually early age strength tests are performed on a panel sprayed at the same time as the tunnel lining. In order to test the actual tunnel lining, the engineer would have to be exposed to the risk of falling ground or shotcrete, and may need special plant or scaffolding for access.

Estimation methods of early-age compressive strength have been proposed, such as maturity methods based on the principle that concrete strength is directly related to both age and evolution of temperature in time, i.e. a relationship between the evolution of temperature and age and the strength development is mathematically established. But surface or embedded temperature measurement using thermocouples or other devices would be difficult in a sprayed concrete lining, and would not remove the safety risks related to access or the drawbacks associated with testing discrete locations. Using a thermal imaging camera enables the engineer to remotely scan the whole sprayed concrete lining from a position of safety, without interfering with plant movements necessary for continuous production.

1.2. Thermal conductivity of concrete

ETC varies depending on the concrete mix, and it also varies with age. Cement hydration [6,7], which is responsible for converting a concrete from a fluid to a rigid, load-bearing and durable solid element, alters the volume fractions and spatial arrangement of solids, liquid, and gases within the concrete during hydration and aging. Thus, thermal conductivity at early age differs from one at mature age. For mature concrete ETC has been widely investigated, generally ranging between 1 and 2.5 W/(m °C) [7]. It can reach even lower values, such as 0.1 W/(m °C), for air-rich concrete [7,8].

The fraction and types of each component material, coupled with ambient conditions, all have been considered as factors affecting ETC [6,7,9,10]. According to research conducted by the Bureau of Reclamation, US Department of the Interior, the type of coarse aggregate is the most important factor [4]. They experimentally investigated the effect of these constituents on ETC for conventional concretes and mortars and found that the types and fractions of aggregates affected the thermal conductivity more than other constituents. The importance of aggregate was corroborated by Kim et al. [11]. ETC of individual common concrete constituent materials is known alone, selected one of which has been shown in Table 1.

Table 1
Thermal conductivity of common concrete materials at 25 °C [12].

Materials	Thermal conductivity (W/(m °C))
Gravels	0.7
Granite	1.73–3.98
Limestone	1.26–1.33
Sand (moist)	0.25–2
Sandstone	1.7
Water	0.58
Air	0.026
Portland cement powder	0.29

Water/cement (w/c) ratio, curing temperature, and other factors have been observed influencing ETC of concretes to different extents. Increasing the w/c ratio decreases the ultimate ETC of concrete as it increases the volume of micropores and subsequently adds to the resistance to heat flow [3,6,13,14]. Ukrainczyk & Matusinović studied the influence of temperature on thermal properties and found the ETC of cement pastes increasing with curing temperature rising from 20 °C to 80 °C [15]. The Hashin-Shtrikman boundary conditions and a simple law of mixtures was successfully applied in their work for estimating thermal properties. The work done by Demirboga showed a reduction of ETC caused by addition of mineral admixtures [16].

Reinforcement by steel fibers has been observed to not only enable a notable impact on concrete strength, toughness and resistance to cracking and spalling [14–19], but also has an influence on the thermal properties of concretes. To a concrete having perlite as main coarse aggregate, the addition of 1.75% mass of wavy steel fibers has been observed to increase the thermal conductivity of concrete by 31.2% [17]. But not all previous studies have observed the same effect; this will be discussed in detail later.

Although many studies have been conducted for conventional concrete, not much is known about the thermal properties of sprayed concrete. Assuming its ETC is the same as for conventional concrete is not a safe assumption because its different composition may have a significant effect on ETC.

Studies measuring ETC of hydrating cement pastes presented changing thermal conductivity with time at early hydration ages and showed some dependency on hydration rate [4,10,11,18]. A cement paste hydrated at the fastest rate and reaching the highest peak temperature had a higher thermal conductivity than that of a fresh cement paste by about 40% and hardened paste by about 30%. The hardened paste had a reaction degree of 55%. In some works, during the first 10 h the ETC of cement pastes increased and then dropped consistently during the following 20 h [14,20]. The biggest drop of 0.5 W/(m °C) occurred with CEM I paste. These results imply that concrete may have a changing thermal conductivity at early age and this may be accentuated in sprayed concrete, which tends to have a higher volume fraction of cement paste than conventional concrete.

2. Thermal conductivity assessment approaches

Thermal conductivity for concretes can be measured directly by generating a controlled heat flow through the tested material in a prescribed direction, to ensure that the boundary conditions agree with theoretical technical assumptions. The current most popular direct experimental measurement methods in use are based on two principles: steady-state and transient state.

2.1. Steady state

Steady state measurement follows from the definition of thermal conductivity. Heat flow is generated within a tested material by heating one of its surfaces using a controllable heater. A temperature gradient can be obtained by measuring the surface temperatures of the two faces of the test sample as shown in Fig. 1. A reference material with known ETC is placed in series with the sample and the temperature difference across its ends is used in the calculation. An axial temperature gradient is established through the stack as heat flows from the upper surface through the test sample to a heat sink. When it reaches thermal equilibrium, the temperature difference across the sample is measured along with output from the heat flux transducer shown in Fig. 1. These values and the pre-measured sample thickness are used to calculate ETC. When the ETC of the transducer material, λ_t, is known, then the thermal conductivity, λ, can be obtained using Eq. (1).

$$\lambda = \frac{\lambda_t \cdot (T_2 - T_3) \cdot L}{A \cdot (T_1 - T_2)} \tag{1}$$

where L is the transmitted thickness; A is the area in a direction normal to the heated surface; T_1, T_2 and T_3 are measured surface temperatures as shown in Fig. 1.

The accuracy of this method depends on whether the test sample is subjected to any external thermal influence, i.e. the test material changing its temperature with time without the action of the heater. However, this cannot be easily satisfied when measuring the thermal conductivity of a hydrating concrete or mortar, especially at their early hydration age when the hydration is exothermic. Moreover, if the test sample is moisturized; a non-uniform moisture distribution is very likely to be caused by temperature difference across the sample. The significance of this influence depends on sample size and the magnitude of the applied temperature difference.

2.2. Transient method

The transient measurement method works by heating samples on a small area of their surface. The heater is a metal sensor which also acts as a temperature detector. An advance of the transient measurement over the steady-state method is that the equilibrium state is unnecessary here. Instead of obtaining a stable value, varying signals are recorded as a function of time. Thus, a major advantage of this technique over the steady-state one is high efficiency. Two prevailing ready-to-use transient measurement techniques are hot wire measurement and hot disk measurement.

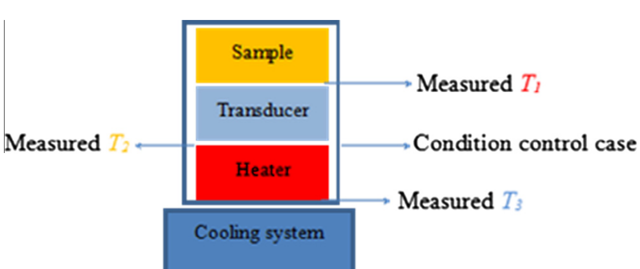

Fig. 1. Schematic set-up for a steady-state thermal conductivity measurement system.

2.2.1. Hot wire method

The conventional hot wire method is a transient dynamic technique based on the measurement of the temperature rise of a thin and straight heat-generating metallic wire (length/radius ratio $\gg$200) embedded in the test material [19,21]. Heat is generated in the wire by passing a constant current through it. When the test sample and wire are at an identical and constant temperature, the temperature rise is measured by a thermocouple and recorded with respect to time during a short heating interval. The ETC of the sample can be calculated from the time-temperature profile as well as the power input by using Eq. (2).

$$\lambda = \frac{Q \cdot ln(t_2/t_1)}{4\pi \cdot (T_2 - T_1)} \tag{2}$$

where T_1 and T_2 are temperatures at times t_1 and t_2, Q is the heat flow per unit time, per unit length of the heating wire.

The hot wire method has been widely used for measuring ETC for porous and highly porous materials and some derivative versions have been created for particular measurement requirements [9,22–25].

2.2.2. Hot disk method

Hot wire methods are especially suitable for measuring ETC in loose samples, while the ETC of consolidated samples is easier to measure by using hot disk methods. Though they are based on the same principle, there is no ready-to-use equipment for the application of hot wire method. Thus, if it is adopted, then a new appliance and a calibration system must be established, which may take much effort to tune it to an adequate degree of accuracy. On the other hand, the hot disk method truly realizes the advantages of the transient plane principle, i.e. rapid and accurate thermal property measurement, which has earned it widespread popularity [26].

Its development began with a non-steady-state method which measured the ETC of a transparent liquid, created by Gustafsson in 1967 [27]. In his work, a thin rectangular metallic foil suspended in the liquid sample was heated by a constant electric current. The temperature distribution around the foil was measured optically as a function of time. From this result, both thermal diffusivity and thermal conductivity of the liquid could be calculated. The advanced hot disk method developed the foil to a flat disk sensor made of a double spiral of electrically conducting nickel wire etched out of a thin foil [28–30]. The wire is 10 μm in thickness. Such a sensor design has two main advantages over the foil sensor. The first is that the wires have much higher resistance than that of the strip, which means that the temperature measurement by measuring the sensor resistance can be performed with higher sensitivity and accuracy [27]. The other advantage is that a much more compact sample can be studied without violating the sample size requirement [27]. This is because in the hot strip method, theoretical analysis assumes that the strip is infinitely long. In practice, it is often required that the length to width ratio is 20:1.

The nickel spiral is situated between two layers of thin polyamide film, Kapton, which provides electrical insulation and

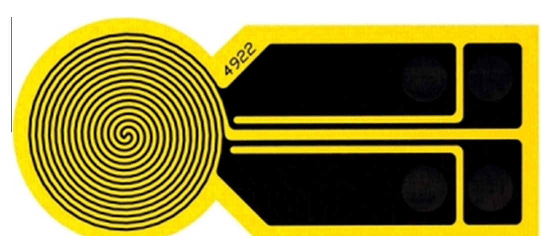

Fig. 2. An example of a flat nickel sensor for hot disk measurement [32].

mechanical stability to the sensor. An example of a proprietary nickel sensor is shown in Fig. 2. A special mathematical computation correlating the thermal conductivity with electronics enable this method to be utilized for obtaining the thermal properties of test materials. It can measure any ETC in the range of 0.01–500 W/(m °C).

During the test, a constant electrical current is passed through the conducting spiral, increasing the sensor temperature and subsequently heating up the adjacent test material. During the measurement, the resistance of the sensor will be recorded as a function of time, and then the recorded resistance data will be transformed into temperature changes of the sensor with time. A mathematical expression has been established to relate the average temperature increase at the sensor surface to the sensor configuration, the output power, and the thermal properties of surrounding materials. Through this expression and the obtained temperature increase of the sensor surface, the thermal properties of the test materials can be calculated. The expression was published in 1990 by Gustafsson, and the mathematical analysis has been extensively reviewed by He more recently [27,31]. Some of the mathematical expressions and analyses are briefly given herein. The temperature changes with time during the test can be worked out by the time-dependent resistance of the sensor according to Eq. (3):

$$R(t) = R_0[1 + \alpha\Delta T(t)] \tag{3}$$

where R_0 ($\approx$5 Ω at room temperature [22]) is the resistance of the sensor element before the transient recording has been initiated; α ($\approx 4.0 \times 10^{-3}$ K^{-1} at room temperature $\approx$298 K [26]) is the temperature coefficient of resistance for the element, and $\Delta T(t)$ is the time-dependent temperature increase of the element.

In other words, the temperature increment $\Delta T(t)$ is associated with the power output of the sensor (P_o), the design parameters of the sensor, and the thermal transport properties of the surrounding sample. For a disk-shaped sensor, the relationship can be expressed as shown in Eq. (4) [31]:

$$\Delta T(\tau) = [P_0/(\pi^{3/2}a\lambda) - 1]D(\tau) \tag{4}$$

where λ is the ETC of tested material, a is the radius of the sensor; and $D(\tau)$ is the theoretical expression of the time-dependent temperature increase which describes the conducting pattern of the sensor. P_o is the power output of the hot disk sensor. The symbol, τ, is a non-dimensional variable created for the sake of simplicity to describe the mean temperature change of the sensor.

The relationship between t and τ is known to be $\tau = (\kappa t/a^2)^{1/2}$. The κ is a known factor, which is the thermal diffusivity of the material. Therefore the temperature change $\Delta T_{(t)}$ can be plotted as a function of $D_{(\tau)}$, and is expected to be a straight line. The slope of the line is $P_o/(\pi^{3/2}a\lambda)$ and so the ETC of λ can be calculated.

Although the mathematical data analysis of the hot disk method is much more complicated than that of other techniques, it is all done automatically by built-in software. The operator only needs to ensure that the sample has been properly prepared for the test, that the sensor has been placed at a proper position on the sample, and that suitable parameters have been input to the running software. The computer-control operation eradicates most of the instrumental errors by the automatic initiation of the system by removing any systematic temperature drift surrounding the sensor and correcting the temperature response time of the sample.

Therefore, compared to other techniques, the hot disk method is rapid and less likely to produce non-uniform moisture distribution in wet samples. The flat sensor means that this technique can substantially reduce the contact resistance between the sample and the sensor. The running time of the measurement is short and controllable. Another advantage of the hot-disk measurement technique is that its measurement flexibility allows the measurement to be easily switched between different surfaces of the sample when needed. Moreover, the influence of moisture content, porosity and density on the thermal conductivity of concrete indicates that the hydration of cement at the expense of water is very likely to induce a changing thermal conductivity with time at early age. Thus, the hot disk measurement technique is the most accurate and flexible technique available for monitoring this variation because of its fast, flexible and effective operation.

2.3. Mathematical estimation methods

Many diverse mathematical approaches are proposed for obtaining ETC. For instance, in Xu & Chung [23], thermal diffusivity, α, for concrete was measured using a laser flash method, a differential scanning calorimeter was used to measure specific heat, and the specific heat capacity was obtained by a differential scanning calorimeter. Subsequently, the ETC of a substance was calculated through the correlation of thermal conductivity with the thermal diffusivity, specific heat capacity, C_p, and density, ρ, according to the correlation between them as shown in Eq. (5).

$$\alpha = \lambda/\rho \cdot C_p \tag{5}$$

Kim et al. established an empirical relationship for thermal conductivity as a function of aggregate volume fraction, fine aggregate fraction, w/c ratio, temperature, and moisture content, as shown in Eq. (6) [11]. All coefficients were determined from individual experimental tests which were designed to analyze the influence of each of the prescribed factors on the thermal conductivity. Thus, this relationship is only suitable for mature concrete composed of similar materials to those used in the study.

$$\lambda_c = \lambda_{ref}[0.293 + 1.01AG][0.8(1.62 - 1.54(W/C)) + 0.2R_h] \times [1.05 - 0.0025T][0.86 + 0.0036(S/A)] \tag{6}$$

where λ_c denotes ETC of concrete, λ_{ref} is a referenced ETC measured from specimens at a condition of $AG = 0.70$, $w/c = 0.4$, $S/A = 0.4$, $T = 20$ °C, and $R_h = 1.0$, AG is the volume fraction of coarse aggregate, S/A is the volume ratio of sand and R_h represents the moisture conditions.

Some of the proposed numerical models for thermal conductivity of multiphase materials may have the potential to be applied to concretes [33–35]. These models take account of various parameters, such as ETC of each constituent phase and individual volume contents, porosity of the material, the shape, the orientation and the distribution of solid particles, and the contact resistance between particles.

A theoretical expression for predicting ETC of highly porous two-phase systems has previously been developed [24]. The porous system was assumed to contain particles of irregular shape dispersed randomly throughout the continuous medium and individual average temperature fields within each phase were used.

The application of most numerical methods are limited either by a requirement for experiments to obtain the parameters for calculation or they are limited to application to similar concretes to the ones the methods have been developed for.

3. Experiments

3.1. Sampling

Concrete cubes of different dimensions were cast from the same batch of concrete. The measurement of thermal conductivity was conducted on two kinds of cubes at the size of 150 mm × 150 mm × 150 mm, one of which contained steel fibers (SFRC) and the other did not (NSFRC). Another 14 cubes at

100 mm × 100 mm × 100 mm with the same materials and fractions but without steel fibers were cast for compressive strength tests, hydration degree tests and density measurement (the results of the former two tests will be presented in another work). The components of the concrete mix are shown in Table 2. All materials were mixed by a vertical mixer and compacted by a vibrating table. The cubes were cured in a waterbath which has been set to 25 °C. The cubes were demoulded at five hours and the measurement followed subsequently.

3.2. Density

As a measure of the compactness of concretes, density directly influences most physical and mechanical properties of concrete. The volume of specimens was obtained from their regular geometric shapes and a balance scale with 0.01 g accuracy measured mass, and then density was calculated from the mass and dimensions.

Furthermore, NSFRC at 20 days was weighed after it had been oven-dried at 80 °C until a constant mass for the later mathematical estimation of its ETC.

3.3. Thermal conductivity measurement

A TPS 2500 S thermal constants analyzer was used to measure ETC of the prepared specimens. The sensor, 29.4 mm (φ) × 0.23 mm (δ), was used. During the test, one of its sides was in contact with sample surface by being placed in the middle of the polished casting surface and the other side was thermally insulated by a 3 cm–thick polystyrene foam board. The running time and running power, which are required to run a test with the equipment, were set to 0.64 ks and 1 W.

3.4. Hydration degree measurement

Several segments from crushed cubes were ground into fine powder, and then sieved through a 0.075 mm mesh to get rid of aggregate particles. The residual cement powder was heated at 60 °C to evaporate free water inside until the powder weight became constant. The weight was recorded as m_1. Subsequently, the powder was heated at 950 °C to decompose hydrated compounds and evaporate the produced moisture until a constant weight which must be recorded as m_2. The same procedure was repeated for the anhydrous cement which has been used for concrete, and then two weights were obtained mc_1 and mc_2 for anhydrous cement. According to Eqs. (7) and (8), hydration degrees can be calculated for each sample.

$$\xi_c = \frac{m_{c1} - m_{c2}}{m_{c2}} \tag{7}$$

$$\xi = \frac{(m_2 - m_1) \times (100 - \xi_c)}{m_2} - \xi_c \tag{8}$$

Table 2
The components of the concrete mix.

	NSFRC	SFRC	Unit
Granite (>0.075 mm & <20 mm)	315	315	kg/m^3
Sand (>0.75 mm & <20 mm)	1255	1255	kg/m^3
CEM I	450	450	kg/m^3
Micro silica fume	50	50	kg/m^3
Steel fiber (35 mm × 1.0 ± 0.03 mm)		30	kg/m^3
Water	211.5	211.5	kg/m^3
Superplasticizer	3.6	3.6	kg/m^3
w/c ratio	0.47	0.47	

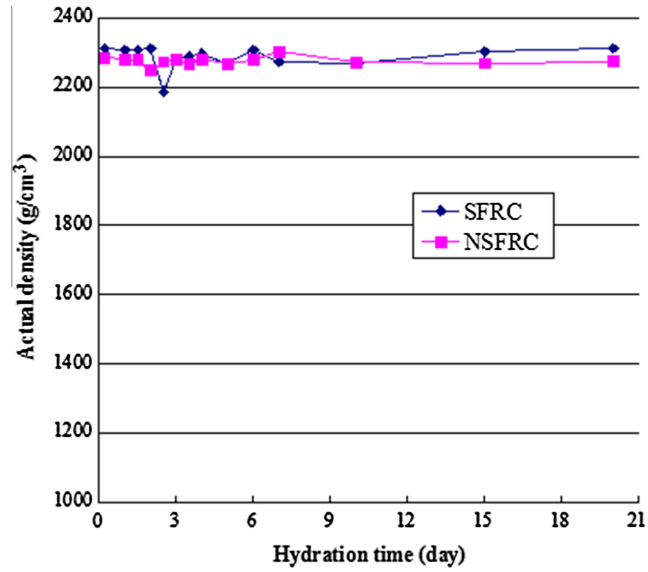

Fig. 3. Density of the SFRC and NSFRC cubes aged from five hours to 20 days.

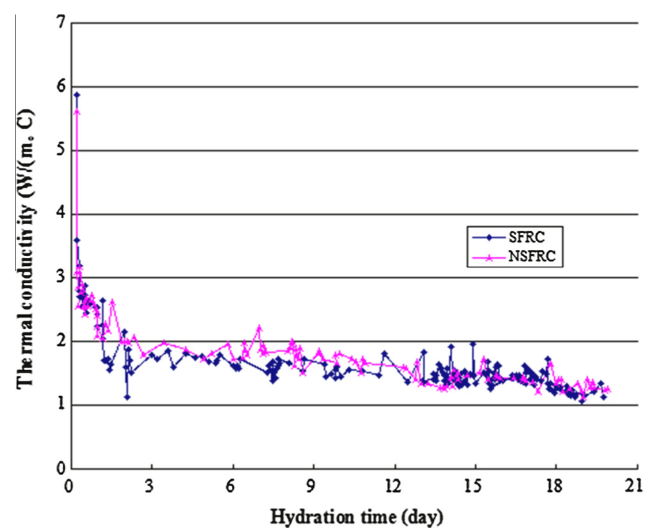

Fig. 4. Thermal conductivity of sprayed concrete aged from five hours to 20 days (SFRC: steel fiber-reinforced sprayed concrete; NSFRC: non-steel reinforced sprayed concrete).

4. Results and discussion

4.1. Density

The density of specimens at ages from five hours to 20 days has been calculated from their mass and dimensions. The SFRC has a mean density of 2287.4 g/cm^3 and the mean density of the specimens without reinforcement (NSFRC) is 2275.1 g/cm^3. The deviation between the values is less than 1%, so it can be considered that the density for both of samples was almost constant during the time period of 20 days, as shown in Fig. 3.

4.2. Thermal conductivity

Fig. 4 shows the data from the tests on the SFRC and NSFRC cubes from five hours after casting to 20 days. It indicates that they both have decreasing ETC with time until a stabilization at which

ETC reaches a value of a similar order to that of mature conventional concretes.

4.3. Effects of reinforcement on thermal conductivity

Based on the data in Fig. 4, the average ultimate ETC was calculated by averaging the data at ages from 18 to 20 days. This was found to be 1.20 ± 0.07 W/(m °C) for SFRC and 1.30 ± 0.09 W/(m °C) for NSFRC. Apparently, NSFRC has a slightly higher thermal conductivity than SFRC.

The SFRC samples contain steel fibers at 1.3% of the total mass of concrete, and NSFRC does not contain any steel. Comparing their thermal conductivity, the difference is about 0.10 W/(m °C), with the NSFRC having a slightly higher value. Although Gül et al.[17] found a significant increase in thermal conductivity when steel fibers were added to concrete at a slightly higher dosage, in many studies, no obvious influence of steel fibers has been observed. For instance, Khaliq and Kodur [25] tested the thermal conductivity of mature self-compacting concrete reinforced by 1.8% by mass steel fiber, which were 38 mm in length and 1.14 mm equivalent diameter, nearly double the length of the steel fibers used in our study. At room temperature, in their work, ETC was 3.5 W/(m °C) for the reinforced concrete and the plain concrete was ETC of 3.3 W/(m °C). Another study on the properties of ultra high performance fiber reinforced concrete reported 0.94 W/(m °C) for the concrete containing steel fibers and 0.98 W/(m °C) for the unreinforced concrete and indicated a similar thermal conductivity between with and without steel fibers units [36]. A surprising result given the dosage was several times higher at 8.1% by mass. Comparing the materials and mix proportions in the present study with these previous studies, the different w/c ratio could be responsible for the different results. The ratio was 0.47 in this study and the ratios for the other two works were less than 0.44.

Fig. 5 demonstrates a random distribution of aggregates and steel fibers within a concrete matrix. Based on the composition of SFRC in this work along with statistical estimation, contact between aggregates and steel fibers is very likely. This occurrence seems leading to increased ETC. However, on microscale, the introduction of steel fibers may introduce internal defects.

It is speculated that the more added water there is, the more water surrounds the steel fibers. As water is consumed by hydration and evaporation, it is replaced not only by hydrated materials but also by pores, voids and cracks [28,37,38]. The process is illustrated in Fig. 6: when the concrete is well-moisturized, the aggregate particles in dark grey and steel fibers in white are surrounded by a thin layer of water in blue; as the moisture content decreases due to hydration and evaporation, pores in black are gradually formed around the grains and fibers in areas originally occupied by water.

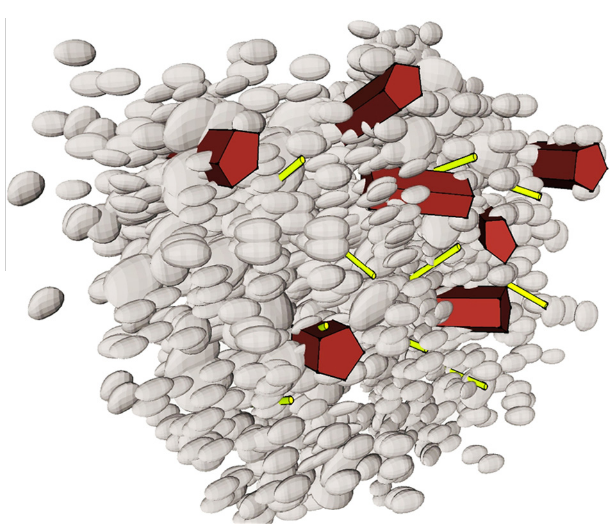

Fig. 5. A distribution model of aggregates and steel fibers within concrete (grey particles represent sand; red grains represents crushed granite aggregate; yellow sticks represent steel fibers). (For interpretation of the references to color in this figure legend, the reader is referred to the web version of this article.)

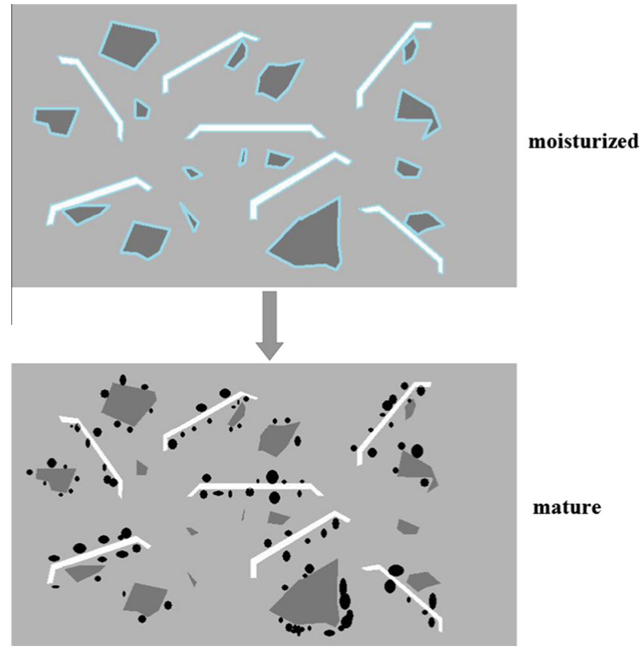

Fig. 6. Illustration of water membrane around aggregate particles and steel fibers inside concrete in an initially moisturized state and the later formation of pores at the original water membrane regions (light grey represents cement paste, sand and micro silica fume; dark grey represents coarse aggregates; white represents steel fibers; light blue represents water membrane; black represents pores.) (For interpretation of the references to color in this figure legend, the reader is referred to the web version of this article.)

Thus, the addition of steel fibers may result in a microstructure with higher porosity and consequently a lower thermal conductivity, unless sufficient steel fibers are added to produce a steel-connected system, which may increase ETC of concrete if the proportion of the cross-sectional area that is steel is significant, or unless steel fibers may be added without a consequent increase in porosity.

4.4. The evolution of thermal conductivity

In Fig. 4, the blue curve represents data for SFRC and the data in pink were from NSFRC. Their values of initial ETC for both stood at a relatively high value, 5.89 W/(m °C) and 5.63 W/(m °C), at the hydration age of five hours. Then, they immediately and sharply dropped until about two days when the curves tended to level up, gradually reaching a constant long-term value. The ETC stabilized at approximately 1.20 ± 0.07 W/(m °C) for SFRC and 1.30 ± 0.09 W/(m °C) for NSFRC.

A concrete system is complicated to start with and its interior structure constantly changes with hydration age. The hydration alters not only volume fractions of solid, liquid and gas phases but also spatial arrangements within the there-dimensional micro-structure. Thus, thermal properties of concrete, such as specific heat capacity, and thermal diffusivity, varying at early age when hydration is very intense, is expected. Heat capacity of composite cement-based materials has been observed to vary with w/c ratios due to the high heat capacity of water (4.18 J/g K), and increase with increasing curing temperature [10]. On the other hand, the opposite trend has been reported for the relationship, but later it has been reported that there is a watershed of water content between these two trends [10,29]. When lower than this watershed, ETC increases with increasing water content, while when higher than it, the trend reverses. The variation of ETC at early age can be explained by the combined effects of thermal diffusivity, α, and heat capacity, C_ρ, as shown by Eq. (9).

$$\alpha = \frac{\lambda}{C_\rho} \tag{9}$$

In another viewpoint, in the course of cement hydration, the concrete gradually turns from a saturated system to a less saturated system because of the loss of water due to cement hydration (the loss of evaporation may be neglected for these samples based on the density data). It has been suggested that the amount of free water in concrete, regardless of density, has a major influence on the ETC [9]. Although water is a poor conductor of heat as compared to rock, it is 25 times more conductive than air [16], which gradually replaces some of the water inside concrete. Further confirmation may be found where studies investigating the influence of curing temperature on ETC of concrete have been explained by the effect of temperature on the evaporation rate of water [25]. Therefore, it is a plausible hypothesis that the evolution of ETC at early age is directly related to variation of moisture content.

After two days, the ETC tended to stabilize, and at the same time, the rate of hydration of the cement was decreasing to a low level. Therefore, the amount of water being consumed by ongoing hydration was too trivial to have a large impact on ETC, though ETC did tend to continue to decrease slowly up to 20 days. The period of relatively constant ETC was about the end of the main period of hydration, Stage III and the beginning of Stage IV. It means all phases of aluminate, ferrite and alite within cement have almost completed their hydration, mainly producing C-S-H gel and calcium hydroxide. The hydration products rapidly deposit into capillary pores, which were originally occupied by mix water. Stage IV is the final stage of hydration, driven by diffusion of water or mineral ions hindered by the thickening layer of hydration products. By then, the interior micro-structure of concrete, such as pore structure and spatial arrangement of solids, will not alter so significantly as before, therefore giving a relatively constant ETC.

4.5. Hydration degrees

The progress of cement hydration has been investigated by a synchronised measurement of hydration degrees at different ages. Fig. 7 shows the growth of hydration degrees of the sample with hydration time. As shown in the graph, the hydration degree exponentially increased with hydration time. During the first two days, the slope of the curve is steep and then becoming closer to a straight line. The fitting of this curve gives Eq. (10) to depict the progress of concrete hydration with time. Comparing this curve to the thermal conductivity curves, the changes of the development trend of these curves almost happened over a same time period.

$$\xi = -7.96 \times exp\left(\frac{t}{2.2}\right) + 14.16 \tag{10}$$

4.6. Simulated thermal conductivity

Theoretically or experimentally establishing a prediction model of ETC for cement-based composite materials has been a focus of research for a long time [11,16,20,29,30,33–36,39–49]. Most empirical or mathematical models consider the influence of coarse aggregates, which have been widely regarded as the main factor, together with moisture content, density, porosity, etc. Models derived from experiments normally give a prediction with good accuracy, such as Kim et al.'s model, which comprehensively considered the dependence on volume fraction of aggregates, w/c ratio, fine aggregate fraction and temperature [11].

There are a lot of prevailing theoretical models for predicting ETC, such as the Campbell-Allen and Thorne models, based on the principle of Ohm's Law, Hamilton and Crosser's model, also based Ohm's law but for porous materials, and the Zimmerman model, which is an advanced version of Hamilton and Crosser's model taking account of pore shapes. However, although these models can all give a satisfactory estimated value, the readily available information pertaining to experimental data and theoretical prediction of the affecting factors related to ETC of concrete is

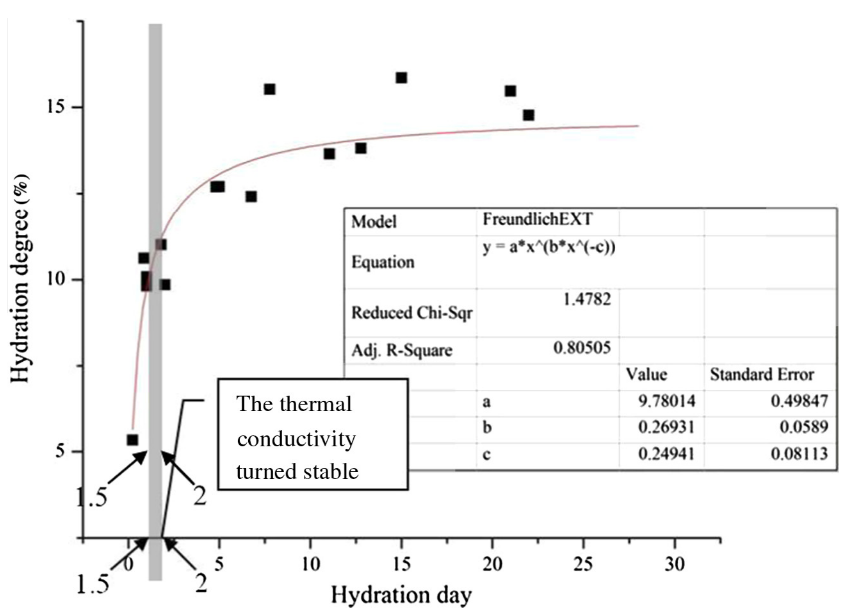

Fig. 7. Hydration degrees of sprayed concrete at various hydration ages.

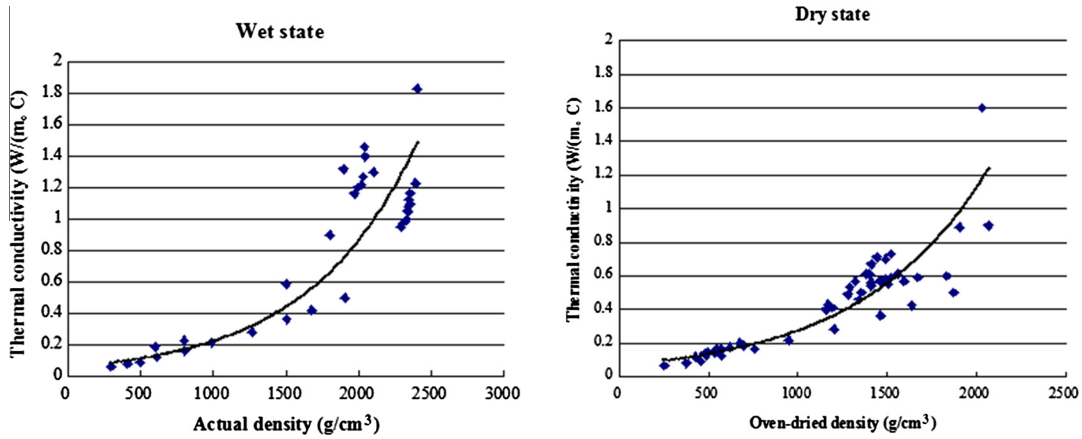

Fig. 8. ETC versus actual density and oven-dried density (data from Table S1).

scarce. Then, experiments are normally required for calibrating and completing the models.

In this work, density and ETC data from different research studies for different concrete materials has been collected and analyzed, as shown in Table S1. The collected data have been classified into two data according to the density information: oven-dried density (ρ_d) and actual density (ρ_a). It was found that, even though these materials consisted of considerably different solid materials, their data are roughly following one trend as shown in Fig. 8 and the extent of the scatter is not considerable. However, the data for the actual density vs thermal conductivity is more scattered than that for the oven-dried density. The cause is the variability of thermal conductivity resulting from uncorrelated moisture content of concrete in different studies due to its high dependence on environmental conditions and other uncontrollable factors, such as temperature and humidity, not only the materials or the hydration process. Thus, the following establishment of simulation method is mainly based on the data from the oven-dried materials.

It has been found more than once that ETC is linearly related with density [30,34,40,50]. On the other hand, in the work in this paper, the relationship between ETC and density, whether it is oven-dried density or wet-state density, is exponential. It is likely to be caused by the varied types of solid materials; however, the linear relationship represents the series of concrete with identical mix materials but with different mixing proportions.

Meanwhile, a regression equation, Eq. (11), was obtained for these data at dry state. When the density in the equation is substituted by measured dry density, then the ETC of the solid part of a concrete system may be estimated. Furthermore, a concrete matrix may be regarded as a three-phase system, as in Woodside and Messimer's work: a solid phase consisting of solid particles of hydrated cement and aggregates, a gas phase consisting of the air voids and a liquid phase consisting of the moisture. In this way, the three-phase model, as shown in Eq. (12), can be used to calculate the overall ETC.

$$\text{Dry state}: \ \lambda_s = 0.059e^{(0.0013\rho_d)} \ R^2 = 0.7828 \tag{11}$$

$$\text{Woodside and Messimer'sthree phase model}: \ \lambda = \lambda_s^{Vs} \cdot \lambda_a^{V_a} \cdot \lambda_w^{V_w} \tag{12}$$

where λ_s is the ETC of the solid part in a concrete; λ_a represents the ETC of air, 0.7 W/(m °C); λ_w is the thermal conductivity of water, 0.58 W/(m °C); V_s, V_a and V_w refer to the volume fraction of each phase.

Table 3
Information of oven-dried density for both crumb-rubber modified concrete in Hall's work and NSFRC in this study, together with the calculated and experimental ETC.

Materials	Oven-dried density (g/cm^3)	Calculated ETC (W/(m °C))	Measured ETC (W/(m °C))
Crumb rubber-modified concrete	2288	1.19	1.269
	2113	1.08	1.069
	2056	0.94	0.8
	1913	0.79	0.686
	2063	1	0.875
	1905	0.85	0.815
	1772	0.69	0.708
	2154	1.1	1.1
	1991	0.92	0.959
	1828	0.82	0.848
NSFRC	2245	1.19	1.29

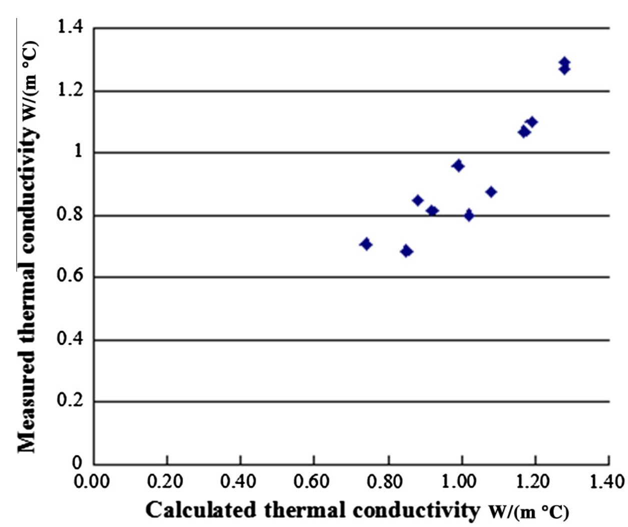

Fig. 9. Calculated ETC values versus that from experiment for both crumb-rubber modified concrete in Hall's work and NSFRC in this study (data from Table 3).

Next, this prediction approach is evaluated by calculating the ETC of the crumb rubber-modified concrete from Hall's work by adopting its data of measured dry density and comparing with their measured ETC [51,52]. There is a good agreement between the calculated and measured values, as shown in Table 3. The same procedure has been repeated for the ETC of NSFRC prepared in this work, which gave an excellent match as shown in Table 3. All of the calculated and measured data has been plotted in Fig. 9, in which a nearly linear relationship indicates an acceptable result. Therefore, it can be considered that ETC of all concrete with the density ranging from 0.2 g/cm^3 to 2.5 g/cm^3, and containing no significant fraction of highly thermally-conductive materials, is in an exponential relationship with density. Moreover, when its density at dry state is known, a rough estimation with an acceptable accuracy can be made, which is particularly convenient and useful for industrial application.

For SFRC in this work, this approach is not suitable as the ETC of steel fibers differ significantly from those of other components.

5. Conclusions

Usually the ETC of concretes are evaluated at an average temperature and are treated as a constant in calculations [49]. However, according to the above results and discussion, the ETC of sprayed concrete at an early stage is much higher than that at a mature age and it experiences an immediate and sharp decrease until two days after which it tends to stabilize. ETC of concrete is confirmed to be changing with hardening. At an early age, the variation of ETC is associated with changes in the free water content and its later stabilization is attributed to the completion of the main and intense hydration of cement, from stage I to III. The ultimate ETC is 1.20 ± 0.07 W/(m °C) for SFRC and 1.29 ± 0.09 W/(m °C) for NSFRC.

Addition of steel fibers at a dosage of 1.4% by mass into the mix does not increase the ETC of concrete. Furthermore, it has been noticed that a higher water content reduces the ETC of concrete when it contains steel fibers because more water magnifies the interfacial effect between steel fiber and solid, causing more defects and higher porosity.

The evolution process of ETC of hardening concrete can be divided into two parts: at early age when cement hydration is intense and the concrete is well moisturized, its ETC mainly varies with the changes of water content; after the end of the intense hydration, micro-structural features, especially density and porosity, are the key determinants.

ETC of all kinds of concrete is exponentially related with density. For concrete with density ranging from 0.2 g/cm^3 to 2.5 g/cm^3 and containing no distinguishable highly-thermal-conductive materials, their ETC can be conveniently estimated from the dry density of concrete, together with the three-phase equation presented in this paper.

Acknowledgments

This project was funded by the Warwick Impact Fund 2011–2015 at the University of Warwick. The work published in this paper was based on experiments undertaken in the concrete and thermodynamic laboratories of the School of Engineering at the University of Warwick and the help of technicians is gratefully acknowledged, in particular Colin Banks. The raw materials were supplied by Normet UK in Coventry. Answers to many queries were provided by the team; in particular Ross Dimmock, Ryan Griffith, and Roar Myrdal.

Appendix A. Supplementary data

Supplementary data associated with this article can be found, in the online version, at http://dx.doi.org/10.1016/j.conbuildmat.2016.07.091.

References

[1] B.D. Jones, Apparatus & method for monitoring strength development of concrete GB. wo/2015/001344, 2014.
[2] B.D. Jones, S. Li, Early strength monitoring of shotcrete using thermal imaging, in: 7th Int. Symp. Sprayed Concr. – Mod. Use Wet Mix Sprayed Concr. Undergr. Support, Sandefjørd, Norway, 2014, pp. 245–254.
[3] K. Kovári, History of the sprayed concrete lining method – part I: milestones up to the 1960s, Tunn. Undergr. Sp. Technol. 18 (2003) 57–69.
[4] Thermal properties of concrete Boulder Canyon Project Final Report, 1940.
[5] Testing Sprayed Concrete – Part 2: Compressive Strength of Young Sprayed Concrete, BS EN 14488-2, 2006.
[6] P. Bamforth, D. Chrisholm, J. Gibbs, T. Harrison, Properties of concrete for use in Eurocode 2: How to optimise the engineering properties of concrete in design to Eurocode 2, 2008.
[7] N. Narayanan, K. Ramamurthy, Structure and properties of aerated concrete: a review, Cem. Concr. Compos. 22 (2000) 321–329, http://dx.doi.org/10.1016/S0958-9465(00)00016-0.
[8] M.C. Nataraja, N. Dhang, A.P. Gupta, Stress–strain curves for steel-fiber reinforced concrete under compression, Cem. Concr. Compos. 21 (1999) 383–390, http://dx.doi.org/10.1016/S0958-9465(99)00021-9.
[9] J.F. Lamond, J.H. Pielert, Thermal properties, in: significance tests prop, Concr. Concr. Mater. (2006).
[10] D.P. Bentz, A review of early-age properties of cement-based materials, Cem. Concr. Res. 38 (2008) 196–204, http://dx.doi.org/10.1016/j.cemconres.2007.09.005.
[11] K.-H. Kim, S.-E. Jeon, J.-K. Kim, S. Yang, An experimental study on thermal conductivity of concrete, Cem. Concr. Res. 33 (2003) 363–371, http://dx.doi.org/10.1016/S0008-8846(02)00965-1.
[12] Thermal conductivity of some common materials and gases, 2013. <http://www.engineeringtoolbox.com/thermal-conductivity-d_429.html>.
[13] J.M. Wong, F.P. Glasser, M.S. Imbabi, Evaluation of thermal conductivity in air permeable concrete for dynamic breathing wall construction, Cem. Concr. Compos. 29 (2007) 647–655, http://dx.doi.org/10.1016/j.cemconcomp.2007.04.008.
[14] B. Milovanovic, I. Banjad Pecur, I. Gabrijel, Measuring thermal properties of hydrating cement pastes, in: 31st Cem. Concr. Sci. Conf. Nov. Dev. Innov. Cem. Mater., London, UK, 2011.
[15] N. Ukrainczyk, T. Matusinović, Thermal properties of hydrating calcium aluminate cement pastes, Cem. Concr. Res. 40 (2010) 128–136, http://dx.doi.org/10.1016/j.cemconres.2009.09.005.
[16] R. Demirboğa, Influence of mineral admixtures on thermal conductivity and compressive strength of mortar, Energy Build. 35 (2003) 189–192, http://dx.doi.org/10.1016/S0378-7788(02)00052-X.
[17] R. Gül, E. Okuyucu, İ. Türkmen, A.C. Aydin, Thermo-mechanical properties of fiber reinforced raw perlite concrete, Mater. Lett. 61 (2007) 5145–5149, http://dx.doi.org/10.1016/j.matlet.2007.04.050.
[18] P. Mounanga, A. Khelidj, G. Bastian, Experimental study and modelling approaches for the thermal conductivity evolution of hydrating cement paste, Adv. Cem. Res. 16 (2004) 95–103.
[19] J.J. Healy, J.J. de Groot, J. Kestin, The theory of the transient hot-wire method for measuring thermal conductivity, Phys. B+C 82 (1976) 392–408, http://dx.doi.org/10.1016/0378-4363(76)90203-5.
[20] P. Mounanga, G. Bastian, A. Khelidj, Experimental study and modeling approaches for the thermal conductivity evolution of hydrating cement paste, Adv. Cem. Res. 16 (2004) 95–103.
[21] B. Merckx, P. Dudoignon, J.P. Garnier, D. Marchand, Simplified transient hot-wire method for effective thermal conductivity measurement in geo materials: microstructure and saturation effect, Adv. Civ. Eng. 2012 (2012) 1–10, http://dx.doi.org/10.1155/2012/625395.
[22] M.B. Suleiman, Thermal conductivity of saturated samples using the hot-disk technique, in: Proc. 4th WSEAS Int. Conf. HEAT Transf. Therm. Eng. Environ., 2006, pp. 140–145.
[23] Y. Xu, D.D.L. Chung, Reducing the drying shrinkage of cement paste by admixture surface treatments, Cem. Concr. Res. 30 (2000) 241–245, http://dx.doi.org/10.1016/S0008-8846(99)00239-2.
[24] R. Jagjiwanram Singh, Effective thermal conductivity of highly porous two-phase systems, Appl. Therm. Eng. 24 (2004) 2727–2735, http://dx.doi.org/10.1016/j.applthermaleng.2004.03.010.
[25] W. Khaliq, V. Kodur, Thermal and mechanical properties of fiber reinforced high performance self-consolidating concrete at elevated temperatures, Cem. Concr. Res. 41 (2011) 1112–1122, http://dx.doi.org/10.1016/j.cemconres.2011.06.012.
[26] D. Mikulic, B. Milovanovic, I. Gabrijel, Analysis of Thermal properties of cement paste during setting and hardening, (n.d.). <https://bib.irb.hr/datoteka/513769.NDTMS-2011_full_paper-Milovanovic-revised.pdf>.
[27] Y. He, Rapid thermal conductivity measurement with a hot disk sensor: Part 1. Theoretical considerations, Thermochim. Acta 436 (2005) 122–129, http://dx.doi.org/10.1016/j.tca.2005.06.026.
[28] A. Michel, A.O.S. Solgaard, B.J. Pease, M.R. Geiker, H. Stang, J.F. Olesen, Experimental investigation of the relation between damage at the concrete-steel interface and initiation of reinforcement corrosion in plain and fibre reinforced concrete, Corros. Sci. 77 (2013) 308–321, http://dx.doi.org/10.1016/j.corsci.2013.08.019.
[29] D. Taoukil, A. El bou, F. Sick, A. Mimet, H. Ezbakhe, T. Ajzoul, Moisture content influence on the thermal conductivity and diffusivity of wood–concrete composite, Constr. Build. Mater. 48 (2013) 104–115, http://dx.doi.org/10.1016/j.conbuildmat.2013.06.067.
[30] M. Bederina, L. Marmoret, K. Mezreb, M.M. Khenfer, A. Bali, M. Quéneudec, Effect of the addition of wood shavings on thermal conductivity of sand

concretes: experimental study and modelling, Constr. Build. Mater. 21 (2007) 662–668, http://dx.doi.org/10.1016/j.conbuildmat.2005.12.008.
[31] S.E. Gustafsson, Transient plane source techniques for thermal conductivity and thermal diffusivity measurements of solid materials, Rev. Sci. Instrum. 62 (1991).
[32] <https://www.researchgate.net/figure/280232534_fig4_Fig-7-Kapton-sensor-used-for-measurements>.
[33] K.J. Kontoleon, T.G. Theodosiou, K.G. Tsikaloudaki, The influence of concrete density and conductivity on walls' thermal inertia parameters under a variety of masonry and insulation placements, Appl. Energy 112 (2013) 325–337, http://dx.doi.org/10.1016/j.apenergy.2013.06.029.
[34] S.-C. Ng, K.-S. Low, Thermal conductivity of newspaper sandwiched aerated lightweight concrete panel, Energy Build. 42 (2010) 2452–2456, http://dx.doi.org/10.1016/j.enbuild.2010.08.026.
[35] L.H. Nguyen, A.-L. Beaucour, S. Ortola, A. Noumowé, Influence of the volume fraction and the nature of fine lightweight aggregates on the thermal and mechanical properties of structural concrete, Constr. Build. Mater. 51 (2014) 121–132, http://dx.doi.org/10.1016/j.conbuildmat.2013.11.019.
[36] V. Corinaldesi, G. Moriconi, Mechanical and thermal evaluation of ultra high performance fiber reinforced concretes for engineering applications, Constr. Build. Mater. 26 (2012) 289–294, http://dx.doi.org/10.1016/j.conbuildmat.2011.06.023.
[37] B. Reddy, Influence of the Steel-Concrete Interface on the Chloride Threshold Level, Imperial College, 2001.
[38] D. Li, J.L. Tao, Y. Yu, Research on the thermal property of lightweight-aggregate-concrete hollow-block wall, Adv. Build. Mater. 250–253 (2011).
[39] B. Belhadj, M. Bederina, Z. Makhloufi, A. Goullieux, M. Quéneudec, Study of the thermal performances of an exterior wall of barley straw sand concrete in an arid environment, Energy Build. 87 (2015) 166–175, http://dx.doi.org/10.1016/j.enbuild.2014.11.034.
[40] R. Demirboğa, Thermal conductivity and compressive strength of concrete incorporation with mineral admixtures, Build. Environ. 42 (2007) 2467–2471, http://dx.doi.org/10.1016/j.buildenv.2006.06.010.
[41] R. Demirboğa, R. Gül, The effects of expanded perlite aggregate, silica fume and fly ash on the thermal conductivity of lightweight concrete, Cem. Concr. Res. 33 (2003) 723–727, http://dx.doi.org/10.1016/S0008-8846(02)01032-3.
[42] R. Demirboga, A. Kan, Thermal conductivity and shrinkage properties of modified waste polystyrene aggregate concretes, Constr. Build. Mater. 35 (2012) 730–734, http://dx.doi.org/10.1016/j.conbuildmat.2012.04.105.
[43] F.M. Díez Ramírez, F.B. Muñoz, E.L. López, A.V. Polanco, Thermal evaluation of structural concretes for construction of biodigesters, Energy Build. 58 (2013) 310–318, http://dx.doi.org/10.1016/j.enbuild.2012.11.036.
[44] A.H.-C. Shin, U. Kodide, Thermal conductivity of ternary mixtures for concrete pavements, Cem. Concr. Compos. 34 (2012) 575–582, http://dx.doi.org/10.1016/j.cemconcomp.2011.11.009.
[45] L.S. Verma, A.K. Shrotriya, R. Singh, D.R. Chaudhary, Prediction and measurement of effective thermal conductivity of three-phase systems, J. Phys. D. Appl. Phys. 24 (1991) 1515. http://stacks.iop.org/0022-3727/24/i=9/a=002.
[46] S. Wei, C. Yiqiang, Z. Yunsheng, M.R. Jones, Characterization and simulation of microstructure and thermal properties of foamed concrete, Constr. Build. Mater. 47 (2013) 1278–1291, http://dx.doi.org/10.1016/j.conbuildmat.2013.06.027.
[47] T.S. Yun, Y.J. Jeong, T.-S. Han, K.-S. Youm, Evaluation of thermal conductivity for thermally insulated concretes, Energy Build. 61 (2013) 125–132, http://dx.doi.org/10.1016/j.enbuild.2013.01.043.
[48] K.-H. Yang, K.-H. Lee, Tests on high-performance aerated concrete with a lower density, Constr. Build. Mater. 74 (2015) 109–117, http://dx.doi.org/10.1016/j.conbuildmat.2014.10.030.
[49] W. Wongkeo, P. Thongsanitgarn, K. Pimraksa, A. Chaipanich, Compressive strength, flexural strength and thermal conductivity of autoclaved concrete block made using bottom ash as cement replacement materials, Mater. Des. 35 (2012) 434–439, http://dx.doi.org/10.1016/j.matdes.2011.08.046.
[50] U. Johnson Alengaram, B.A. Al Muhit, M.Z. bin Jumaat, M.L.Y. Jing, A comparison of the thermal conductivity of oil palm shell foamed concrete with conventional materials, Mater. Des. 51 (2013) 522–529, http://dx.doi.org/10.1016/j.matdes.2013.04.078.
[51] M.R. Hall, K.B. Najim, C.J. Hopfe, Transient thermal behaviour of crumb rubber-modified concrete and implications for thermal response and energy efficiency in buildings, Appl. Therm. Eng. 33–34 (2012) 77–85, http://dx.doi.org/10.1016/j.applthermaleng.2011.09.015.
[52] K.B. Najim, M.R. Hall, Mechanical and dynamic properties of self-compacting crumb rubber modified concrete, Constr. Build. Mater. 27 (2012) 521–530, http://dx.doi.org/10.1016/j.conbuildmat.2011.07.013.